

# Multifractality of the kicked rotor at the critical point of the Anderson transition

Panayotis Akridas-Morel,<sup>1</sup> Nicolas Cherroret,<sup>1</sup> and Dominique Delande<sup>1,\*</sup>

<sup>1</sup>Laboratoire Kastler Brossel, Sorbonne Université, CNRS,  
ENS-PSL Research University, Collège de France, 4 Place Jussieu, 75005 Paris, France

We show that quantum wavepackets exhibit a sharp macroscopic peak as they spread in the vicinity of the critical point of the Anderson transition. The peak gives a direct access to the multifractal properties of the wavefunctions and specifically to the multifractal dimension  $d_2$ . Our analysis is based on an experimentally realizable setup, the quantum kicked rotor with quasi-periodic temporal driving, an effectively 3-dimensional disordered system recently exploited to explore the physics of the Anderson transition with cold atoms.

In the vicinity of the critical point of a continuous phase transition, large fluctuations are observed [1], responsible for dramatic phenomena like e.g. critical opalescence. Beyond mean-field descriptions, renormalization group approaches make it possible to describe critical phenomena at (almost) all scales, and to predict critical exponents [2]. Large fluctuations arise as well in quantum phase transitions, where they are usually probed via correlation functions or transport properties. The metal-insulator Anderson transition, taking place in disordered quantum systems, is especially interesting. It separates a metallic phase at weak disorder, where transport is diffusive, and an insulating phase at strong disorder, where transport is inhibited due to interference in multiple scattering from random defects [3, 4], a phenomenon known as Anderson localization. The dimensionality of the system is a crucial parameter: Anderson localization is the generic scenario in one-dimensional (1D) systems, while the Anderson transition can be observed in dimension strictly larger than two. In three-dimensional (3D) systems, the critical point of the Anderson transition occurs for strong disorder, when the product of the wavenumber  $k$  with the mean free path  $\ell$  is close to unity,  $(k\ell)_c \approx 1$  [5]. Although the order parameter for the Anderson transition remains debated [6], there is nowadays a wide consensus that it is a second order continuous transition, with an algebraic divergence of the localization length on the localized side,  $\xi \propto 1/((k\ell)_c - k\ell)^\nu$ , and an algebraic vanishing of the diffusion coefficient on the diffusive side,  $D \propto (k\ell - (k\ell)_c)^s$ . Numerous evidence for these properties have been found in numerical simulations of the standard Anderson model, which has been also used to compute the critical exponents  $\nu = s = 1.57$  in dimension  $d = 3$  [7, 8]. This value is universal (depending only on the dimension and symmetry properties and has been confirmed on other models [9]). Numerical studies of the Anderson model have shown that the distribution of conductance at the critical point is universal as well, scale invariant [10] and broad, a clear-cut manifestation of large fluctuations at the critical point. Large fluctuations also show up in the critical eigenstates, which are strongly multifractal, displaying regions where  $|\psi|^2$  is

unexpectedly large and regions where it is unexpectedly small [11]. Usually, this property is quantitatively described using the generalized inverse participation ratio (GIPR) [12, 13]:

$$P_q = \int_{L^d} d^d \mathbf{r} |\psi(\mathbf{r})|^{2q}, \quad (1)$$

where  $q$  is a real number and  $L$  is the system size. The multifractality analysis studies how the GIPR averaged over eigenstates and/or disorder realizations scales with  $L$ . If the average  $\langle P_q \rangle$  scales like  $L^{-\tau_q}$ ,  $\tau_q$  is called the multifractal exponent. By construction  $\tau_0 = -d$  and, by normalization of the wavefunction,  $\tau_1 = 0$ . One can equivalently use the set of multifractal dimensions  $d_q = \tau_q/(q-1)$ . A wavefunction delocalized over a set of dimension  $\mathcal{D}$  (which can be an ordinary or a fractal set) will have  $d_q = \mathcal{D}$  for all  $q$ . For multifractal states, finally,  $d_q$  is a continuous function of  $q$  with large positive  $q$  values probing the regions of large  $|\psi|^2$  and negative  $q$  the regions where  $|\psi|^2$  is vanishingly small.

How to experimentally access multifractal dimensions is far from obvious. This in principle requires to measure wavefunctions for various disorder realizations or energies close to the critical point *everywhere* in space, a tremendously difficult task. Alternatively, one can extract only a part of the information on multifractality by selective, less complete, measurements [14–16], for example of the intensity distribution on the exit plane of a disordered slab. In this Letter, we show that tracing the average expansion of a 1D wavepacket makes it possible to directly measure the multifractal dimension  $d_2$  of a 3D critical system. We base our analysis upon an experimentally existing system, the quasi-periodically kicked rotor (QPKR), which has been shown to display the Anderson metal-insulator transition [17, 18], but the mechanism to extract a multifractal dimension from the expansion of a wavepacket is quite general and could be used in other critical systems.

The QPKR is a spatially 1D system whose dimensionless Hamiltonian depends on time:

$$H = \frac{p^2}{2} + K \cos x [1 + \varepsilon \cos \omega_2 t \cos \omega_3 t] \sum_{n=0}^{N-1} \delta(t-n), \quad (2)$$

where  $K, \varepsilon, \omega_2, \omega_3$  are dimensionless parameters. Provided  $\omega_2, \omega_3, \pi, \hbar$  are mutually incommensurate real numbers, the quantum dynamics of the QPKR has been shown in [19] to be strictly equivalent to an anisotropic 3D Anderson model, where  $K$  controls the disorder strength and  $\varepsilon$  the anisotropy [20], a fact further confirmed by a low-energy effective field theory [21]. An important property of the QPKR is that the localized/delocalized dynamics takes place *in momentum space*, not in position space like the usual Anderson model. Specifically, the system is localized at small  $K$  value (i.e.  $\langle p^2(t) \rangle$  tends to a constant at long  $t$ ) and diffusive at large  $K$  value (i.e.  $\langle p^2(t) \rangle \propto t$  at long  $t$ ). In between, there is a critical point, whose position can be approximately predicted by a mean-field approach, the self-consistent theory of localization (SCTL) [20, 22], where the system behaves sub-diffusively:  $\langle p^2(t) \rangle \propto t^{2/3}$  at long  $t$ . Experimentally, these properties have been confirmed by monitoring the temporal expansion of a wavepacket initially localized in momentum space around  $p = 0$ , that is by measuring  $|\psi(p, t)|^2$  at increasing time, with the initial state  $|\psi(p, 0)|^2 \approx \delta(p)$ . At the critical point, the spatial fluctuations of the wavepacket have been numerically and theoretically studied [23, 24] from an analysis of GIPRs, Eq. (1): they display only very weak multifractal properties at the critical point. In this Letter, we show that the average density  $\langle |\psi(p, t)|^2 \rangle$  itself presents a direct, macroscopic signature of the multifractality of the 3D critical model.

Because of sub-diffusion at the critical point, the width of the wavepacket increases like  $t^{1/3}$ , but its global shape is independent of time, a manifestation of scale invariance. The SCTL makes a definite prediction for this shape [25, 26]:

$$\langle |\psi(p, t)|^2 \rangle = \frac{3}{2} \left( 3\rho^{3/2}t \right)^{-1/3} \text{Ai} \left[ \left( 3\rho^{3/2}t \right)^{-1/3} |p| \right], \quad (3)$$

where  $\rho = \Gamma(2/3)\Lambda_c/3$  is related to the critical quantity  $\Lambda_c = \lim_{t \rightarrow \infty} \langle p^2 \rangle / t^{2/3}$ , a numerical factor depending on the anisotropy  $\varepsilon$  [20], with  $\Gamma$  the Gamma function and  $\text{Ai}(x)$  the Airy function. It is convenient to define scaled variables:  $\mathcal{P} = pt^{-1/3}$ ,  $\mathcal{N}(\mathcal{P}, t) = t^{1/3} \langle |\psi(p, t)|^2 \rangle$  so that:

$$\mathcal{N}(\mathcal{P}) = \frac{3^{2/3}}{2\rho^{1/2}} \text{Ai} \left( \frac{|\mathcal{P}|}{3^{1/3}\rho^{1/2}} \right). \quad (4)$$

This prediction has been found in excellent agreement with the experimental results on the atomic QPKR [25], describing both the kink around  $p = 0$  and the tail  $\propto \exp(-\alpha|\mathcal{P}|^{3/2})$ . In Fig. 1, we show the numerically computed  $\mathcal{N}(\mathcal{P})$  at various times (number of kicks) [27]. While the agreement with Eq. (4) is excellent at short time (100 kicks, comparable to the duration of the experiment), a sharp peak near  $p = 0$  develops at increasingly long times. We show below that this peak - not described

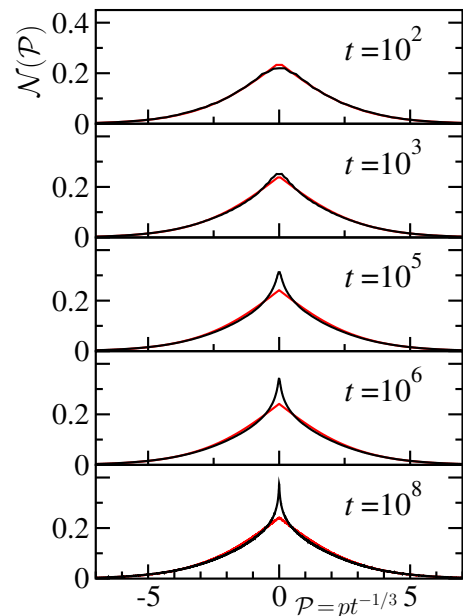


FIG. 1. Temporal evolution in momentum space of a wavepacket launched at  $t=0$ . The numerical simulation (in black) is performed for the quasi-periodically kicked rotor at the critical point of the 3D Anderson transition. The global expansion is sub-diffusive in momentum space  $\langle p^2(t) \rangle \propto t^{2/3}$ . When plotted vs. rescaled coordinate  $\mathcal{P} = pt^{-1/3}$ , the density in momentum space  $\mathcal{N}$  takes a time-independent shape - predicted to be a Airy function, Eq. (3) (red curve) - except near the origin where a sharp peak grows with time. This peak is a direct manifestation of multifractality at the critical point. Parameters are  $K = 8.096, \varepsilon = 0.4544, \omega_2 = 2.67220902067011, \omega_3 = 2.01719090924681, \hbar = 3.54$ .

by the SCTL - is a manifestation of multifractality at the critical point and is directly related to the multifractal dimension  $d_2$ .

To understand the origin of this sharp peak, it is easier to leave the QPKR for a moment and turn back to a standard disordered system such as the Anderson model, where 3D localization takes place in configuration space. The average expansion of a wavepacket with time is described by the disorder-averaged intensity propagator  $P(\mathbf{r}, t)$ , which gives the average probability to move from the origin at  $t = 0$  to  $\mathbf{r}$  at time  $t$  [28]. It is convenient to consider its temporal and spatial Fourier transform  $P(\mathbf{q}, \omega) = \int dt d^d\mathbf{r} P(\mathbf{r}, t) e^{i\omega t - i\mathbf{q}\cdot\mathbf{r}}$ , which can always be written as:

$$P(\mathbf{q}, \omega) = \frac{1}{-i\omega + D(\mathbf{q}, \omega)q^2}. \quad (5)$$

Eq. (9) defines the momentum and frequency dependent diffusion coefficient  $D(\mathbf{q}, \omega)$ . Symmetry properties - discussed in the Supplemental Material [29] - imply that  $D$  depends only on the modulus of  $\mathbf{q}$  and that  $D(\mathbf{q}, i\omega)$  is a real quantity for real  $\omega$ .

Of particular interest is the small  $\omega$  limit of  $D(\mathbf{q}, \omega)$ ,

which describes long times. In this limit and in a usual diffusive system,  $D(q, \omega) = D_0 = \ell^2/(3\tau)$  equals the classical diffusion coefficient, where  $\ell$  is the mean free path and  $\tau = m\ell/\hbar k$  the mean free time. In a localized system,  $D(q, \omega) = -i\omega\xi^2$ , with  $\xi$  the localization length. At the critical point finally, the SCTL predicts  $D(q, \omega) \propto (-i\omega)^{1/3}$  [30, 31], which yields Eq. (3). In turn, deviations from the Airy shape, as visible in Fig. 1, imply that  $D(q, \omega)$  must deviate from the simple  $(-i\omega)^{1/3}$  dependence. In [32], Chalker proposed that, at short distance (large  $q$ ),  $D(q, \omega)$  acquires a non-trivial  $q$ -dependence that we now discuss.  $D(q, \omega)$  must respect the one-parameter scaling law characterizing the Anderson transition at large distance and long time [33]. This scaling law involves the following relevant length scales: the mean free path  $\ell$ ,  $1/q$ , and  $L_\omega = \ell(\omega\tau)^{-1/3}$ , the mean distance traveled by a particle in time  $1/\omega$  at the critical point. The localization length  $\xi$  is in general an additional characteristic length, but at the critical point it is infinite and thus irrelevant. In the following, we will only consider the long time limit  $\omega\tau \ll 1$ , so that  $L_\omega \gg \ell$ . The one-parameter scaling law implies that  $q$  can enter in  $D(q, \omega)$  only through the  $qL_\omega$  combination. Under this constraint, Chalker's ansatz [34] distinguishes the three following regimes [32, 35]:

- (A) When  $qL_\omega < 1$  (long distance), multifractal correlations have no time to develop and one expects the normal sub-diffusive behavior, i.e.  $D(q, i\omega) \propto D_0(\omega\tau)^{1/3}$ . This is region (ii) in [32].
- (B) When  $qL_\omega > 1$  (short distance), but still  $q\ell < 1$ , multifractality sets in and  $D$  takes a  $q$  dependence:  $D(q, i\omega) \propto D_0(\omega\tau)^{1/3}(qL_\omega)^{d_2-2}$ , where  $1 < d_2 < 2$ . This is region (v) in [32].
- (C) Finally, at very short distance  $q\ell > 1$ , the mean free path sets a non-universal cut-off preventing the divergence of  $D$  so that  $D(q, i\omega) \propto D_0(\omega\tau)^{1/3}(L_\omega/\ell)^{d_2-2}$ . While (A) and (B) obey the one-parameter scaling law, regime (C) breaks it at short distance where no (sub)-diffusive behavior makes sense. This is region (iv) in [32].

Using these forms, it is simple to deduce the scaling of the intensity propagator [36]. Especially, in the ‘‘multifractal’’ (B) region where  $\ell < r < L_{\omega=1/t}$ , one finds [37, 38]:

$$P_{3D}(\mathbf{r}, t) \propto t^{-d_2/3} r^{d_2-3}. \quad (6)$$

Numerical simulations on the Anderson model [36] have confirmed the existence of the scalings (A-C).

How can we relate the laws (A-C) to the observed behavior for the QPKR? The mapping between the 1D QPKR and a 3D spatially disordered system relies on a projection of the 3D dynamics onto a 1D axis. This is obtained by considering states and wavepackets which are entirely delocalized in fictitious 2D planes transverse to

the axis  $x$  of the kicked rotor where the actual 1D dynamics takes place, for details see [19]. This means that, instead of the 3D intensity propagator  $P_{3D}(\mathbf{r}, t)$ , one has to consider its projection  $\Pi(x, t) = \int P((x, y, z), t) dy dz$ . In the mean-field sub-diffusive regime (A), performing the integration over  $x$  and  $y$  leads to the Airy function, Eq. (3) [29, 39]. For the multifractal regime (B), one obtains the following short distance behavior:  $\Pi(x, t) = t^{-1/3} [\alpha - \beta |xt^{-1/3}|^{d_2-1}]$ . The  $\alpha, \beta$  constants are not universal and depend on the boundary around  $qL_\omega = 1$  between the normal sub-diffusive and the multifractal regions (A) and (B), but the algebraic dependence  $|xt^{-1/3}|^{d_2-1}$  is universal. Note that because  $d_2 \approx 1.24$ , the 3D intensity propagator, Eq. (6), has an algebraic divergence near  $r = 0$  while its projection  $\Pi(x)$  is finite at  $x = 0$ , with an algebraic singularity.

In addition to the spatial projection, two additional peculiarities of the QPKR must be taken into account. First, the localization takes place in momentum space instead of configuration space, so that  $p$  should be substituted to  $x$ . Second, the classical diffusion is anisotropic. This requires to introduce an anisotropic diffusion tensor [40], but it turns out that after projection along the two transverse directions the spatio-temporal scaling of the wavefunction remains valid [29], so that, eventually:

$$\mathcal{N}(\mathcal{P}) = \alpha - \beta |\mathcal{P}|^{d_2-1}, \quad (7)$$

at small  $\mathcal{P}$ . While the contribution of the mean-field regime (A) to  $D(q, \omega)$  leads to the kink  $\mathcal{N}(\mathcal{P}) - \mathcal{N}(0) \propto |\mathcal{P}|$  at small  $\mathcal{P}$  (see Eq. (4)), the multifractal law (14) is more singular: it is responsible for the small peak near the origin observed in Fig. 1. At short time (say shorter than 100 kicks), this rather weak singularity at the origin is cut at the mean free path, and the normal component (the Airy function) reproduces very well the numerical calculation. As time grows, the whole wavepacket spreads in size like  $t^{1/3}$ , making the short distance cut-off to act at smaller and smaller  $\mathcal{P} = pt^{-1/3}$ . Note that because  $d_2 > 1$ , the algebraic term in Eq. (14) does not diverge at  $\mathcal{P} = 0$ , only its derivative is infinite.

We can now use the numerically computed wavepackets to extract the value of the multifractal dimension  $d_2$ . We have used two different methods [29], see Fig. 2. In the first one, we simply fit the central part of the wavepacket with the expression (14), excluding distances smaller than the mean free path (regime (C)). This method gives consistently a value of  $d_2$  in the [1.24, 1.32] range for a considerably large time interval, between  $10^3$  and  $4 \times 10^8$  kicks, in good agreement with the known value  $1.24 \pm 0.015$  for the 3D Anderson model [11, 41]. In the second method, we use for  $D(q, \omega)$  a form that smoothly interpolates between the three regimes (A-C) (sub-diffusive at large distance, multifractal at short distance, non-universal at very short distance), and numerically compute the expected shape of the wavepacket. The details of the fitting procedure are discussed in [29]. We

found that the fitted  $d_2$  is almost insensitive to the details of the interpolation between the three regimes. For  $t = 10^6$  kicks, the two methods give almost identical results,  $d_2 = 1.28$ , and the quality of the fits is excellent, as shown in Fig. 2. The Airy function, in contrast, strongly deviates from the numerical result.

We finally show in Fig. 3 that the same value of  $d_2$  allows to reproduce almost perfectly the full momentum distribution over a very wide range of times. The fact that a unique form of  $D(q, \omega)$  reproduces the numerical results over more than 6 orders of magnitude of  $t$  is on the one hand a very strong hint that the one-parameter scaling law remains valid for the Anderson transition in the multifractal regime, and on the other hand a confirmation of the validity of the Chalker's ansatz.

Note that an apparently similar phenomenon, an enhanced return probability, has been recently experimentally observed on the kicked rotor [42]. It originates from the constructive interference between pairs of time-reversed paths for time-reversal invariant systems and is *completely different* from the "multifractal" peak: it manifests itself on a much shorter spatial scale of the order of the mean free path, that is in regime (C) where the one-parameter scaling law is violated. Moreover, it exists only for *periodic* driving, as discussed in [42, 43] and is thus an unrelated phenomenon.

In conclusion, we have unveiled the existence of a sharp multifractality peak at the critical point of the Anderson transition. Based on the the equivalence between the time-dependent QPKR and the 3D anisotropic Anderson model, we have also shown that the multifractal dimension  $d_2$  of a critical 3D system can be extracted from the peak in the frame of a 1D experimental setup. Although this in principle requires to reach extremely long times, we stress that, even after  $t = 10^3$  kicks – a value already reached in state-of-the-art experiments [44] – a significant deviation from the Airy shape is already visible. This opens the way to an experimental measure of multifractality properties using the atomic kicked rotor. The method proposed in this Letter is in no way restricted to the kicked rotor and could be used in other disordered systems [14]. In a full 3D system, the average intensity propagator, Eq. (6), is also sensitive to  $d_2$ . If not all three dimensions of space are experimentally accessible, averaging over one or two dimensions still preserves the information on  $d_2$ , although the singularity is somewhat smoothed out.

We thank G. Lemarié, J.C. Garreau, P. Szriftgiser, A. Mirlin and V.E. Kravstov for useful discussions. This work was granted access to the HPC resources of TGCC under the allocation 2013-056089 made by GENCI (Grand Equipement National de Calcul Intensif) and to the HPC resources of The Institute for scientific Computing and Simulation financed by Region Ile de France and the project Equip@Meso (reference ANR-10-EQPX- 29-01).

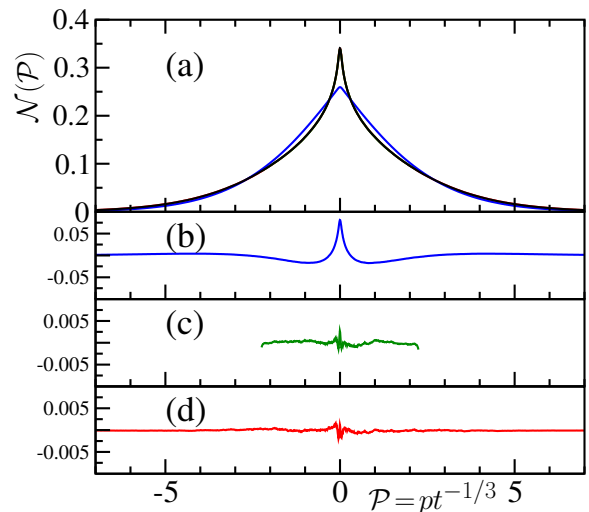


FIG. 2. (a) Black curve: Numerically computed temporal evolution at  $10^6$  kicks in momentum space of a wavepacket launched at  $t = 0$  near momentum  $p = 0$  (see Fig. 1 for the parameter values). The fit by an Airy function, Eq. (3), blue curve, which does not take into account multifractality, is obviously bad; The residual (difference between the curve and the best fit) is shown in (b). The central region is very well fitted by an algebraic dependence, Eq. (14), (residual shown in (c)) and gives  $d_2 = 1.28 \pm 0.03$  (note the vertical scale 10 times smaller than in (b)). A fit of the full numerical curve interpolating between the three regimes (A-C) and in particular incorporating the multifractal regime (B) is indistinguishable from the numerical result, and gives  $d_2 = 1.28 \pm 0.02$ ; The residual is shown in (d).

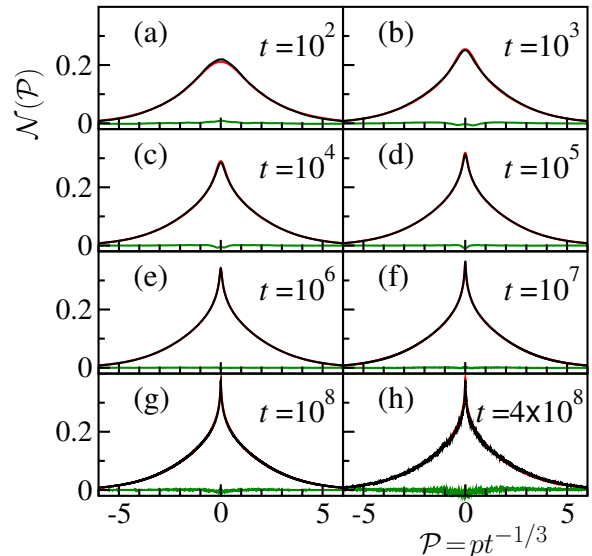


FIG. 3. Black solid lines: numerically computed temporal evolution in momentum space of a wavepacket launched at  $t = 0$  near momentum  $p = 0$  (see Fig. 1 for the parameter values). Red lines: prediction taking into account the sub-diffusive dynamics and the multifractality of the eigenstates (regimes (A-C)). The agreement is excellent (residuals are displayed as green curves) over more than 6 decades of time. The same value  $d_2 = 1.26$  has been used for all plots.

- \* Corresponding author: Dominique.Delande@lkb.upmc.fr
- [1] L. Landau, E. Lifshitz, and L. Pitaevskii, *Statistical Physics*, Course of theoretical physics (Butterworth-Heinemann, 1980).
- [2] K. G. Wilson, *Rev. Mod. Phys.* **55**, 583 (1983).
- [3] P. W. Anderson, *Phys. Rev.* **109**, 1492 (1958).
- [4] P. A. Lee and T. V. Ramakrishnan, *Rev. Mod. Phys.* **57**, 287 (1985).
- [5] A. F. Ioffe and A. R. Regel, in *Progress in semiconductors*, Vol. 4, edited by A. F. Gibson (London : Heywood, 1960) pp. 237–291.
- [6] F. Evers and A. D. Mirlin, *Reviews of Modern Physics* **80**, 1355 (2008).
- [7] K. Slevin and T. Ohtsuki, *New Journal of Physics* **16**, 015012 (2014).
- [8] K. Slevin and T. Ohtsuki, *J. Phys. Soc. Jpn.* **87**, 094703 (2018).
- [9] S. Ghosh, D. Delande, C. Miniatura, and N. Cherroret, *Phys. Rev. Lett.* **115**, 200602 (2015), 1506.08116.
- [10] P. Markos, *Europhysics Letters (EPL)* **26**, 431 (1994).
- [11] A. Rodriguez, L. J. Vasquez, K. Slevin, and R. A. Römer, *Phys. Rev. B* **84**, 134209 (2011).
- [12] R. J. Bell and P. Dean, *Discussions of the Faraday Society* **50**, 55 (1970).
- [13] C. Castellani and L. Peliti, *Journal of Physics A: Mathematical and General* **19**, L429 (1986).
- [14] S. Faez, A. Strybulevych, J. H. Page, A. Lagendijk, and B. A. van Tiggelen, *Phys. Rev. Lett.* **103**, 155703 (2009).
- [15] A. Richardella, P. Roushan, S. Mack, B. Zhou, D. A. Huse, D. D. Awschalom, and A. Yazdani, *Science* **327**, 665 (2010).
- [16] M. Mascheck, S. Schmidt, M. Silies, T. Yatsui, K. Kitamura, M. Ohtsu, D. Leipold, and E. Runge, *Nature Photonics* **6**, 293 (2012).
- [17] J. Chabé, G. Lemarié, B. Grémaud, D. Delande, P. Szriftgiser, and J. C. Garreau, *Phys. Rev. Lett.* **101**, 255702 (2008).
- [18] M. Lopez, J.-F. Clément, P. Szriftgiser, J. C. Garreau, and D. Delande, *Phys. Rev. Lett.* **108**, 095701 (2012).
- [19] G. Lemarié, J. Chabé, P. Szriftgiser, J. C. Garreau, B. Grémaud, and D. Delande, *Phys. Rev. A* **80**, 043626 (2009).
- [20] M. Lopez, J.-F. Clément, G. Lemarié, D. Delande, P. Szriftgiser, and J. C. Garreau, *New J. Phys* **15**, 065013 (2013).
- [21] C. Tian, A. Altland, and M. Garst, *Phys. Rev. Lett.* **107**, 074101 (2011).
- [22] D. Vollhardt and P. Wölfle, in *Electronic Phase Transitions*, edited by Hanke, W. and Kopaev Yu. V. (Elsevier, 1992) pp. 1–78.
- [23] J. Martin, I. García-Mata, O. Giraud, and B. Georgeot, *Phys. Rev. E* **82**, 046206 (2010).
- [24] I. García-Mata, J. Martin, O. Giraud, and B. Georgeot, *Phys. Rev. E* **86**, 056215 (2012).
- [25] G. Lemarié, H. Lignier, D. Delande, P. Szriftgiser, and J. C. Garreau, *Phys. Rev. Lett.* **105**, 090601 (2010).
- [26] G. Lemarié, *Transition d'Anderson avec des ondes de matière atomiques*, Ph.D. thesis, Université Pierre et Marie Curie, Paris (2009).
- [27] Formulas such as Eq. (3) are valid for the average intensity, and this implies an averaging over realizations of the disorder. For a single realization, one expects additional fluctuations. For the QPKR, a fully deterministic system, disorder averaging is replaced by averaging over the phases of the  $\omega_2, \omega_3$  quasiperiodic excitations [19]. Additionally, one can average over the quasi-momentum along the  $x$  direction, in a Brillouin zone.
- [28] Technically, the propagator  $P(\mathbf{r}_1, \mathbf{r}_2, \omega) = \overline{G^R(\mathbf{r}_1, \mathbf{r}_2, E + \omega/2)G^A(\mathbf{r}_2, \mathbf{r}_1, E - \omega/2)}/2\pi n$  is proportional to the disorder average of the product of retarded and advanced Green's functions at energy  $E$ , with  $n$  the density of states per unit volume. Thanks to the statistical translational invariance of the disorder, it depends only on  $\mathbf{r} = \mathbf{r}_1 - \mathbf{r}_2$ . For simplicity of the notations in the main text, we write only  $\mathbf{r}$  and omit the  $E$ -dependence of quantities.
- [29] See Supplemental Material at [URL will be inserted by publisher], for details on the symmetry properties of  $D(q, \omega)$ , the application of the self-consistent theory of localization to the kicked rotor and the fitting procedures used to determine the multifractal exponent  $d_2$ .
- [30] B. Shapiro, *Phys. Rev. B* **25**, 4266 (1982).
- [31] C. A. Müller and D. Delande, “Disorder and interference: localization phenomena,” (Oxford Scholarship, 2011) Chap. 9, ArXiv:1005.0915.
- [32] J. Chalker, *Physica A* **167**, 253 (1990).
- [33] E. Abrahams, P. W. Anderson, D. C. Licciardello, and T. V. Ramakrishnan, *Phys. Rev. Lett.* **42**, 673 (1979).
- [34] In [32], a fourth regime, labeled (iii), is introduced between the normal and the multifractal regimes, with  $D(q, i\omega) \propto q$ . We tried to add it in our fits, but the quality of the results was much worse. We thus conclude that this regime does not actually exist.
- [35] T. Brandes, B. Huckestein, and L. Schweitzer, *Annalen der Physik* **508**, 633 (1996).
- [36] B. Huckestein and R. Klesse, *Phys. Rev. B* **59**, 9714 (1999).
- [37] F. J. Wegner, *Zeitschrift für Physik B Condensed Matter* **25**, 327 (1976).
- [38] V. E. Kravtsov, O. M. Yevtushenko, P. Snajberk, and E. Cuevas, *Phys. Rev. E* **86**, 021136 (2012).
- [39] I. S. Gradshteyn and I. M. Ryzhik, *Table of integrals, series, and products*, 5th ed. (Elsevier/Academic Press, Amsterdam, 1994).
- [40] G. Lemarié, D. Delande, J. C. Garreau, and P. Szriftgiser, *J. Mod. Opt.* **57**, 1922 (2010).
- [41] L. Vasquez, *High precision multifractal analysis in the 3D Anderson model of localisation*, Ph.D. thesis, University of Warwick, Warwick (2010).
- [42] C. Hainaut, I. Manai, R. Chicireanu, J.-F. Clément, S. Zemmouri, J. C. Garreau, P. Szriftgiser, G. Lemarié, N. Cherroret, and D. Delande, *Phys. Rev. Lett.* **118**, 184101 (2017).
- [43] C. Hainaut, I. Manai, J.-F. Clément, J. C. Garreau, P. Szriftgiser, G. Lemarié, N. Cherroret, D. Delande, and R. Chicireanu, *Nat. Commun.* **9**, 1382 (2018).
- [44] I. Manai, J.-F. Clément, R. Chicireanu, C. Hainaut, J. C. Garreau, P. Szriftgiser, and D. Delande, *Phys. Rev. Lett.* **115**, 240603 (2015).

## Supplemental Material

### SYMMETRY PROPERTIES OF THE MOMENTUM AND FREQUENCY DEPENDENT DIFFUSION COEFFICIENT

In this section, we discuss the symmetry properties of the disorder-averaged intensity propagator, Eq. (5) of the main text, for a system of dimension  $d$  in the presence of a disordered potential, whose statistical properties are transitionally and rotationally invariant.

The disorder-averaged intensity propagator  $P(\mathbf{r}_1, \mathbf{r}_2, t)$  gives the average probability to move from position  $\mathbf{r}_1$  at  $t = 0$  to  $\mathbf{r}_2$  at time  $t$ . Because the disordered potential is statistically homogeneous and isotropic, it depends only on the distance  $|\mathbf{r}_1 - \mathbf{r}_2|$ . It is convenient to consider its temporal and spatial Fourier transform  $P(\mathbf{q}, \omega) = \int dt d^d \mathbf{r} P(\mathbf{r}, 0, t) e^{i\omega t - i\mathbf{q} \cdot \mathbf{r}}$ , which depends only on the modulus  $|q|$  and can be written as:

$$P(\mathbf{q}, \omega) = \frac{1}{-i\omega + D(q, \omega)q^2}. \quad (8)$$

which defines the momentum and frequency dependent diffusion coefficient  $D(q, \omega)$ .

Causality implies that  $P(\mathbf{r}_1, \mathbf{r}_2, t)$  vanishes for negative  $t$ , while unitarity of the Hamiltonian evolution implies the conservation of probability  $\int P(\mathbf{r}_1, \mathbf{r}_2, t) d^d \mathbf{r}_2 = 1$  for all  $t > 0$ . This implies, after Fourier transformation:

$$P(0, \omega) = \frac{1}{-i\omega}. \quad (9)$$

Thus,  $D(q, \omega)$  has no singularity in the upper complex half-plane  $\Im \omega > 0$  and cannot diverge more rapidly than  $1/q^2$  at small  $q$ .

Because  $P(\mathbf{r}_1, \mathbf{r}_2, t)$  is a real function, its Fourier transform satisfies:

$$P(q^*, \omega^*) = P^*(q, -\omega) \quad (10)$$

where the  $*$  denotes complex conjugation, so that;

$$D(q^*, \omega^*) = D^*(q, -\omega) \quad (11)$$

In particular,  $D(q, i\omega)$  must be real for real  $q, \omega$ .

### SPECIFICITIES OF THE KICKED ROTOR

In this section, we explain how the general framework developed for 3D disordered systems can be adapted to the quasi-periodically kicked rotor described by Hamiltonian (2) of the main text.

The equivalence between the QPKR and a 3D disordered system is described in details in [19]. An initial

1D wavepacket of the QPKR can be mapped on a initial state of the equivalent 3D disordered system which is completely delocalized - i.e. with a uniform density - over the two transverse  $y, z$  directions. During the temporal evolution, this complete transverse delocalization is preserved, so that average intensity 1D propagator can be obtained from the 3D one simply by averaging over the transverse directions. In Fourier space, this means that only  $q_y = q_z = 0$  contributes. In [40], it has been shown that the 3D equivalent system is anisotropic so that the disorder-averaged propagator can be written as:

$$P(\mathbf{q}, \omega) = \frac{1}{-i\omega + \mathbf{q} \cdot \mathbf{D}(\mathbf{q}, \omega) \cdot \mathbf{q}}. \quad (12)$$

where  $\mathbf{D}$  is the anisotropic diffusion tensor. Because the 1D propagator of the QPKR involves only  $q_y = q_z = 0$ , the only component that matters is  $D_{xx}$ , so that everything boils down to the simpler isotropic case.

### SINGULARITY OF THE DISORDER-AVERAGED INTENSITY PROPAGATOR NEAR THE ORIGIN

The behavior of the disorder-averaged intensity propagator near the origin  $x = 0$  is a bit subtle at the critical point. We first consider the non-multifractal case where the diffusion coefficient  $D(q, \omega)$  scales like  $\omega^{1/3}$ . We use the mixed momentum-time representation of the intensity propagator:

$$P(\mathbf{q}, t) = \int d^d \mathbf{r} P(\mathbf{r}, 0, t) e^{-i\mathbf{q} \cdot \mathbf{r}} = \frac{1}{2\pi} \int d\omega P(\mathbf{q}, \omega) e^{i\omega t} \quad (13)$$

At very large  $q$ , the  $-i\omega$  term in the denominator of Eq. (9) can be neglected and the integral over  $\omega$  computed exactly, e.g. using Eq. 3.761.9 in [39]. The result is  $\propto q^{-2}t^{-2/3}$ . The  $1/q^2$  behavior at large distance implies, after a 3D Fourier transform, a  $1/r$  divergence in configuration space.

In the specific case of the kicked rotor we are interested in, the Fourier transform has to be performed only along a single direction and momentum  $p$  has to be substituted to position  $x$  (see section above). As a result, the  $1/q^2 t^{2/3}$  behavior at large distance now implies a  $|p|/t^{2/3}$  singularity in the intensity propagator  $P(p, t)$ . The next term is a constant scaling like  $t^{-1/3}$ , in accordance with the one-parameter scaling law, finally leading to  $\mathcal{N}(\mathcal{P}) \approx \alpha - \beta|\mathcal{P}|$  at small  $\mathcal{P} = pt^{-1/3}$ . In fact, it is possible to perform exactly the full double Fourier transform, see [25, 26]. The result is Eq. (4) of the main text, which displays explicitly the expected linear singularity near the origin.

When the multifractal regime comes into play,  $D(q, \omega)$  scales like  $q^{d_2 - 2}\omega^{1 - d_2/3}$  at large  $q$  (regime (B) in the main text). Again, the  $-i\omega$  term in the denominator of Eq. (9) can be neglected and the integral over  $\omega$  computed exactly. The result is  $\propto q^{-d_2}t^{-d_2/3}$ . After a 3D Fourier

transform, this gives the  $r^{d_2-3}t^{-d_2/3}$  divergence of Eq. (6) of the main text. In the specific case of the kicked rotor, the 1D Fourier transform gives a  $|p|^{d_2-1}/t^{d_2/3}$  singularity near  $p = 0$ , that is Eq. (7) of the main text. Because  $1 < d_2 < 2$ , the singularity due to the multifractal component dominates at small  $p$ , explaining the origin of the sharp peak.

## FITTING PROCEDURE

As explained in the main text, two different fitting procedures have been used, in order to extract the multifractal dimension  $d_2$  from numerical experiments.

### Numerical calculation of the disorder-averaged intensity propagator

The structure of the Hamiltonian, Eq. (2) of the main text, makes it very easy to numerically propagate any initial state. The free evolution operator between two consecutive kicks is diagonal in the momentum eigenbasis, while the instantaneous kick operator is diagonal in the position eigenbasis. Because the Hamiltonian is spatially periodic with period  $2\pi$ , we use the Bloch theorem which makes it possible to restrict to a configuration space  $x \in [0, 2\pi[$  with periodic boundary conditions, changing only the kinetic energy term in the Hamiltonian  $p^2/2$  to  $(p + \hbar\beta)^2/2$ , where  $\beta \in ]-1/2, 1/2[$  is the Bloch vector. The configuration space,  $x \in [0, 2\pi[$ , is discretized in  $N$  equidistant points; in momentum space, this corresponds to wavevectors (that is, up to multiplicative factor  $\hbar$ , momenta) in the  $] -N/2, N/2[$  range. Passing between configuration and momentum space involves a Fourier transform of length  $N$ , (the dimension of the Hilbert space) which can be done efficiently.

Altogether, the propagation algorithm is thus a series of forward and backward Fourier transforms interleaved with multiplication of each component of the current state by a phase factor. The initial state is chosen as a  $\delta$  function at the origin  $\psi(p, t=0) = \delta(p)$ . The quantity  $|\psi(p, t)|^2$  is thus the intensity propagator at time  $t$ . The averaging over disorder realizations is performed firstly by averaging over many values of the Bloch vector  $\beta$ , and secondly by averaging over the phases of the quasi-periodic kick amplitude modulation, i.e. by adding two random phases  $\phi_2, \phi_3$  in Eq. (2) of the main text:  $\cos(\omega_2 t + \phi_2) \cos(\omega_3 t + \phi_3)$ . We explored a third possibility: shifting the initial state at a non-zero initial momentum  $\psi(p, t=0) = \delta(p - p_0)$ , which is also an efficient averaging, although not used in the data presented in this paper. It is also possible to use a slightly broadened wavepacket in momentum space (for example a Gaussian) as initial state. It results in a slightly smoothed disorder-averaged intensity propagator. At long time

where the subdiffusion leads anyway to a broad disorder-averaged intensity propagator, it makes no significant difference. After averaging  $|\psi(p, t)|^2$  over the disorder realizations, we obtain the disorder-averaged intensity propagator  $P(p, t)$ . As explained in the main text, a simple rescaling of the momentum  $p$  to  $\mathcal{P} = pt^{-1/3}$  provides us with the quantity  $\mathcal{N}(\mathcal{P}, t) = t^{1/3}P(p, t)$ , displayed in Figs. 1 to 3 of the main text.

The size  $N$  of the Hilbert space must be chosen sufficiently large for the momentum distribution to the negligibly small at the maximum momentum  $|p| = N\hbar/2$ . We used up to  $N = 49152$  for the longest time considered  $t = 4 \times 10^8$ . The averaging was performed over 17600 disorder realizations for times up to  $t = 10^6$ , 8800 for  $t = 10^7$ , 1536 for  $t = 10^8$  and 120 for  $t = 4 \times 10^8$ .

### First fitting procedure

The first fitting procedure uses only the very central part, near  $p = 0$ , of the numerically computed disorder-averaged intensity propagator. Indeed, Eq. (7) of the main text predicts an algebraic cusp at small  $\mathcal{P}$  :

$$\mathcal{N}(\mathcal{P}) = \alpha - \beta|\mathcal{P}|^{d_2-1}, \quad (14)$$

clearly visible at long times. We thus fitted the central part of the numerically computed  $\mathcal{N}(\mathcal{P}, t)$  with Eq. (14), with three fitting parameters  $\alpha, \beta$  and  $d_2$ . The range of  $\mathcal{P}$  values used must be not too large, as the fitting expression is expected to be valid only near  $\mathcal{P} = 0$ . We chose to include points up to  $|\mathcal{P}| = 2.25$  - see the green curve in Fig. 2(c) of the main text - but the extracted  $d_2$  value turns out to depend only weakly on the range used. This simple procedure already gives very satisfactory results, with values of  $d_2$  almost independent of time at long time, although a separate fit is done for each time.

At very short  $p$ , of the order of the mean free path, the disorder-averaged intensity propagator does not obey the one-parameter scaling law of the Anderson transition (regime (C) in the main text), so that the expression (14) is not expected to be valid. In other words, the algebraic cusp at small  $p$  is smoothed over one mean free path. The corresponding range in  $\mathcal{P} = pt^{-1/3}$  shrinks when  $t$  increases, explaining why the peak near  $p = 0$  grows. Such a smoothing affects the quality of the fit. In order to take this fact into account, we have used two different strategies. The first option is to exclude a small region around  $\mathcal{P} = 0$  from the fit. The second option is to use a phenomenological smoothing by convoluting Eq. (14) with a Gaussian:

$$g(p) = \frac{1}{\ell\sqrt{2\pi}} \exp\left(-\frac{p^2}{2\ell^2}\right) \quad (15)$$

where  $\ell$  is a constant (independent of time) of the order of the mean free path. Both strategies give similar results.



In Table I, we give the values of  $d_2$  extracted from the numerical data, for various times. The uncertainties take into account the fluctuations of the results when the range of  $\mathcal{P}$  used for the fit is varied, and the fluctuations when the size of the small region near the origin is varied (first option) or when  $q_0$  is varied (second option).

Time $t$	$10^3$	$10^4$	$10^5$	$10^6$	$10^7$	$10^8$	$4 \times 10^8$
$d_2$	1.37	1.33	1.31	1.28	1.26	1.26	1.26
$\Delta d_2$	0.15	0.05	0.04	0.03	0.02	0.02	0.02

TABLE I. Multifractal exponent  $d_2$ , with estimated uncertainty  $\Delta d_2$ , extracted from fits of the disorder-averaged intensity propagator near momentum  $p = 0$  by Eq. (14), for various times  $t$ . The uncertainty is not the statistical error bar of the fit, but rather reflects the fluctuations of the result of the fit when the momentum range and the short-range cutoff are varied. Nevertheless, the result at long times is remarkably stable, proving the robustness of the fitting procedure.

### Second fitting procedure

The second fitting procedure uses the full numerically computed disorder-averaged intensity propagator. It assumes that the momentum-frequency dependent diffusion coefficient follows the Chalker's ansatz [32] with the three different regimes presented in the main text. More precisely, we use the following ansatz:

$$D(q, i\omega) = \frac{3}{2^{2/3}} D_0 (\omega\tau)^{1/3} f(qL_\omega) \quad (16)$$

where  $\tau$  is the mean scattering time,  $D_0 = \ell^2/3\tau$  the classical Boltzmann diffusion coefficient ( $\ell$  is the mean free path) and  $L_\omega = \ell(\omega\tau)^{1/3}$  is the mean distance traveled at the critical point in time  $1/\omega$ . The fact that the real function  $f$  depends only on the product  $qL_\omega$  is a requirement of the one-parameter scaling law. In the non-multifractal regime (A) where  $qL_\omega \ll 1$ , the self-consistent theory of localization predicts that  $f$  is constant [20]. The precise constant value of  $f$  depends on the cut-offs used in the self-consistent theory [20, 22, 31]. If the cut-off is chosen so that the transition takes place at  $k\ell = 1$ , the numerical factors in Eq. (16) are such that  $f = 1$  in the non-multifractal regime.

In the multifractal regime  $qL_\omega > 1$ , the Chalker's ansatz [32] states that  $D(q, i\omega)$  scales like  $q^{d_2-2}\omega^{1-d_2/3}$  of, equivalently,  $f(qL_\omega) \propto (qL_\omega)^{d_2-2}$ . There are of course many possibilities to smoothly connect the  $f(x) = 1$  behavior at small  $x$  to the  $f(x) \propto x^{d_2-2}$  decrease at large  $x$ . The only requirement is that the transition between the two regimes takes place around  $x = 1$ . In order to avoid unphysical Gibbs-like oscillations after Fourier

transform, we used the following smooth ansatz:

$$f(x) = \left[ 1 + (x/x_0)^{\gamma(2-d_2)} \right]^{-1/\gamma} \quad (17)$$

where  $\gamma$  is a positive exponent and  $x_0$  a number of the order of unity characterizing the transition point between the two regimes. This ansatz is of course a bit arbitrary. We have tried a few other ways of smoothly connecting the two regimes, which give very similar final results. When the parameters  $D_0, \tau, d_2, x_0, \gamma$  are given,  $D(q, i\omega)$  is entirely specified. In order to compute the disorder-averaged intensity propagator, one has to compute  $D(q, \omega)$  for real  $\omega$ , which is rather easy by analytic continuation in the complex plane, as there is no singularity in the upper half-plane  $\Im\omega > 0$ . The last step is a double Fourier transform from  $q, \omega$  to  $x, t$  to obtain  $P(x, t)$ . In order to take into account the non-universal behavior at very short distance (below the mean free path, regime (C) for  $D(q, \omega)$  in the main text), we convolute the obtained  $P(x, t)$  by a Gaussian, Eq. (15). We use these distributions to fit the numerical results obtained for the kicked rotor. There are 5 different fit parameters: the first one is the "classical" diffusion coefficient  $D_0$  which determines the overall scaling factor of the distribution (or equivalently the value of  $\langle p^2 \rangle / t^{2/3}$  at long time); Taking  $D_0$  as a fit parameter accounts for the somewhat arbitrary numerical prefactor in Eq. (16), not accurately predicted by the self-consistent theory. The second fit parameter is the short distance cutoff  $\ell$  in Eq. (15), of the order of the mean free path. It turns out that the final results are essentially insensitive to the exact value of this parameter. The three left important parameters are  $d_2$  (the figure of merit of our analysis), and  $x_0, \gamma$  which describe the transition between the normal and multifractal regimes for  $D(q, \omega)$ . We performed three fitting runs:

- In the first run, we fit all five parameters  $D_0, \tau, d_2, x_0, \gamma$  for each time. We observed that the values of  $x_0$  and  $\gamma$  fluctuate in not too large intervals, that is  $x_0 \in [0.24, 0.40]$  and  $\gamma \in [2.8, 4.0]$ .
- In a second run, we fix  $\gamma$  at its most probable value  $\gamma = 3.0$  and fit the remaining four parameters.
- In a third run, we additionally fix  $x_0$  at its most probable value  $x_0 = 0.3$  and fit the remaining three parameters.

The results of the three fitting runs are very similar. Importantly, the residuals of the fits - deviations between the numerical data and the fitting functions - are very comparable for the three runs, so that they are of almost equal significance. The fluctuations of the fitted values for the three runs give an estimate of the error due the imperfections of the fits. Combined with the statistical uncertainty of the fit, they provide a reasonable estimate



of the error bars on the determined values of  $d_2$ . These values are given in Table II. They are more or less time-independent at long time, which strongly supports the validity of the Chalker's ansatz. They also agree well with the results of Table I and with the known value [11] of the multifractal dimension  $d_2 = 1.24 \pm 0.015$  (a more accurate value  $d_2 = 1.243 \pm 0.006$  is given in the unpublished thesis [41]).

Time $t$	$10^2$	$10^3$	$10^4$	$10^5$	$10^6$	$10^7$	$10^8$	$4 \times 10^8$
$d_2$	1.19	1.32	1.34	1.33	1.28	1.25	1.24	1.24
$\Delta d_2$	0.2	0.2	0.08	0.04	0.02	0.015	0.015	0.01

TABLE II. Multifractal exponent  $d_2$ , with estimated uncertainty  $\Delta d_2$ , extracted from fits of the disorder-averaged intensity propagator for various times  $t$ . The uncertainty is the combination of the statistical error bar of the fit and of the three different values that are obtained when the additional parameters  $q_0, \gamma$  are either fitted or fixed. In any case, the smallness of  $\Delta d_2$  as well as the quality of the fit - see Fig. 2 of the main text - validates the Chalker's ansatz and proves that it is experimentally possible to measure the multifractal exponent  $d_2$ .